

ANALYSIS OF CRACK INITIATION AND PROPAGATION IN POLYCRYSTALLINE MESO- AND MICROSTRUCTURES OF METAL MATERIALS

Torsten Luther¹ and Carsten Könke²

¹ Institute of Structural Mechanics
Marienstrasse 15, 99421 Weimar, Germany
e-mail: torsten.luther@bauing.uni-weimar.de

² Institute of Structural Mechanics
Marienstrasse 15, 99421 Weimar, Germany
e-mail: carsten.koenke@bauing.uni-weimar.de

Keywords: Polycrystal Model, Grain Size Distribution, Damage Analysis.

Abstract. *Meso- and microscale analysis are promising disciplines to cover the crack initiation as well as the various crack propagation phenomena in engineering structures. On mesoscale it is observed that the crack propagation in polycrystalline metal materials occurs mainly along grain boundaries. Following this observation we present a two dimensional polycrystal meso model consisting of grains with an elastic orthotropic material law and cohesive interfaces along crystal boundaries, which is able to reproduce crack initiation and propagation in metallic materials. As an extension to classical Voronoi cell diagrams we apply an advanced algorithm to generate polycrystal material structures based on arbitrary distribution functions of grain size. Therewith we are more flexible to represent realistic grain size distributions. The polycrystal model is applied to analyze the crack initiation and propagation in statically loaded representative volume elements of aluminum on the mesoscale without the necessity of initial damage definition. Future research work is focused on the determination of constitutive relations for the cohesive interface law from mixed continuum atomistic simulations performed on a representative volume element on the microscale and homogenized to the mesoscale.*

1 INTRODUCTION

Durability and life cycle analysis of engineering structures is often based on numerical simulations of macroscopic damage behavior using phenomenological damage and fracture models. Therewith the true physical mechanisms of crack initiation and various crack propagation can not be covered. In order to integrate the physical material effects, which are leading to crack initiation as well as crack propagation, simulations on the meso- or microstructure have to be performed.

For metallic polycrystals we can observe, that crack initiation and propagation on the mesoscale ($10^{-3}\text{m} - 10^{-6}\text{m}$) occurs mainly along grain boundaries and depends strongly on atomic debonding on the microscale ($10^{-6}\text{m} - 10^{-10}\text{m}$). The mutual dependence can be investigated by a multiscale analysis obtaining a reasonable damage model based on micro mechanical features. The current work is focused on the investigation of damage behavior on the mesoscale using a two dimensional polycrystal model. Fundamentals of polycrystal modeling on mesoscale are published by Iesulauro and Ingraffea [1-3]. We will refer to this publications later in the course of generation of geometry and assignment of material models.

In section 2 we describe an algorithm to generate polycrystalline material structures based on arbitrary defined grain size distributions. Section 3 gives an overview of the material models, which are assigned to grains and grain boundaries. Section 4 shows numerical results of mesoscopic damage analysis on representative volume elements (RVE) of aluminum. In section 5 we introduce the mixed continuum atomistic model of Tadmor et al. [4] on the microscale to simulate atomic debonding along grain boundaries. The intention is to determine the constitutive relations of grain boundary decohesion on the mesoscale by homogenization of a RVE on the microscale. Finally section 6 concludes the current work.

2 GENERATION OF POLYCRYSTALLINE MATERIAL STRUCTURE

The application of 'classical' Voronoi algorithms [5] to generate polycrystalline material structures has become state of the art in polycrystal modeling on the mesoscale. The advantage of a Voronoi cell diagram, as applied in [1-3], is given by its computational simplicity and random characteristics. However, Voronoi cell diagrams are not well adapted to reproduce a realistic grain size distribution in metallic polycrystals. Experimental measurements in polycrystal materials have found, that in steady state the grain size distribution is better fit by a lognormal distribution function [6,7] or a Weibull distribution function [8]. Exemplary, Figure 1 shows cumulative grain size distribution in heat treated thin layer aluminum measured by [6] and compared to the Voronoi grain size distribution and the lognormal distribution. In grain size distribution functions the size of a single grain is defined by the diameter d of its circle with equivalent area. The plotted cumulative lognormal distribution function is computed with the measured median value $d_{50} = 0.94 \mu\text{m}$ and the measured standard deviation $\sigma_d = 0.78$ [6]. The Voronoi grain size distribution was calculated by means of generated Voronoi cell diagrams with the same median value.

Based on the drawn conclusion we modified the 'classical' Voronoi algorithm to generate more realistic two dimensional grain structures of polycrystals. Our concept is to predefine the size of single grains according to a specified grain size distribution and to construct a 'modified' Voronoi cell diagram considering this a priori information. In the following we apply the lognormal distribution function as starting point for the grain structure generation. The lognormal distribution function, $f_{LN}(d)$, is given as:

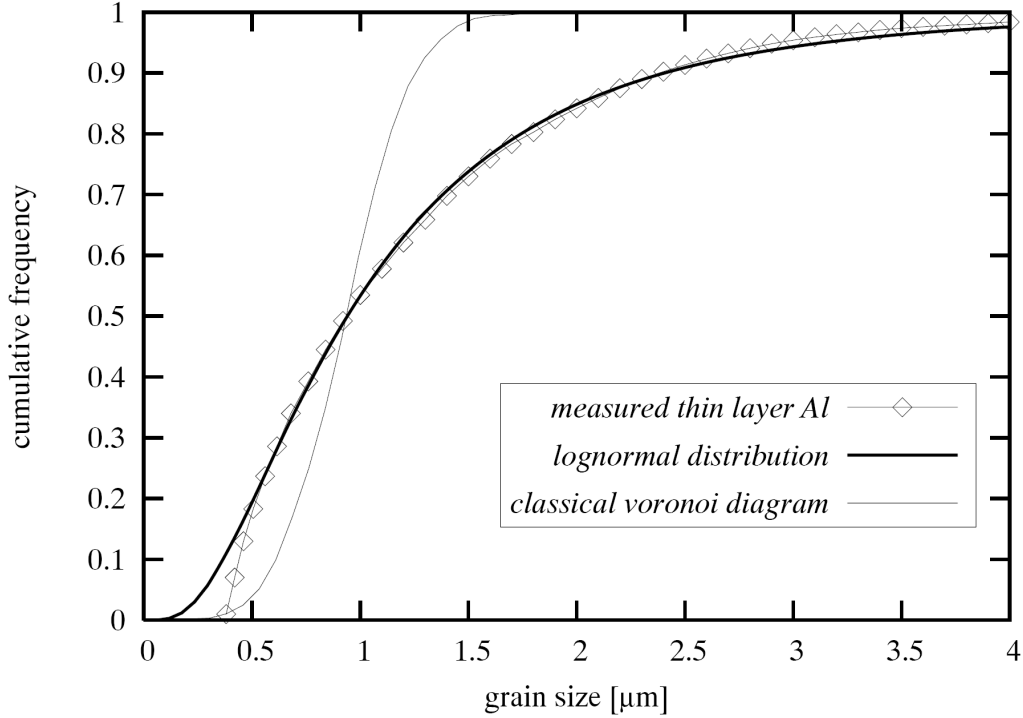


Figure 1: Cumulative grain size distribution.

$$f_{LN}(d) = \frac{1}{\sigma_d d \sqrt{2\pi}} e^{-\left(\frac{1}{\sqrt{2}\sigma_d} \ln(d/d_{50})\right)^2}, \quad (1)$$

where the median grain size d_{50} and the standard deviation σ_d are the free parameters. Alternatively a Weibull distribution $f_W(d)$ is defined by the two free parameters α and β :

$$f_W(d) = \frac{\beta}{\alpha^\beta} d^{\beta-1} e^{-(d/\alpha)^\beta}. \quad (2)$$

The main advantage of the lognormal distribution function is the straightforward interpretation of its free parameters, which is not given in the case of Weibull distribution.

In a first step the grain structure generation starts with a random generation of diameters d according to the specified distribution function. In the case of a Weibull distribution we are able to transform the cumulative distribution function $F_W(d)$:

$$F_W(d) = 1 - e^{-(d/\alpha)^\beta} \quad (3)$$

into the form:

$$d = \alpha \{-\ln(1 - F_W(d))\}^{1/\beta}. \quad (4)$$

Therewith we can find a suitable set of diameters d based on random values $0 < F_W(d) < 1$. For distribution functions, that can not be transformed into a dependency $d = d(F(d))$, e.g. the lognormal distribution, we discretize the argument domain $0 < d \leq d_{max}$ of the distribution function $f(d)$. The discretization yields a finite number of discrete intervals $\Delta d_i = d_{i+1} - d_i$. Furthermore we assign the probability limits $F(d_i) < F(\Delta d_i) \leq F(d_{i+1})$ to each step Δd_i according to the cumulative distribution function $F(d)$. Therewith we can generate a suitable set of diameters d based on random values $0 < F(d) \leq F(d_{max})$.

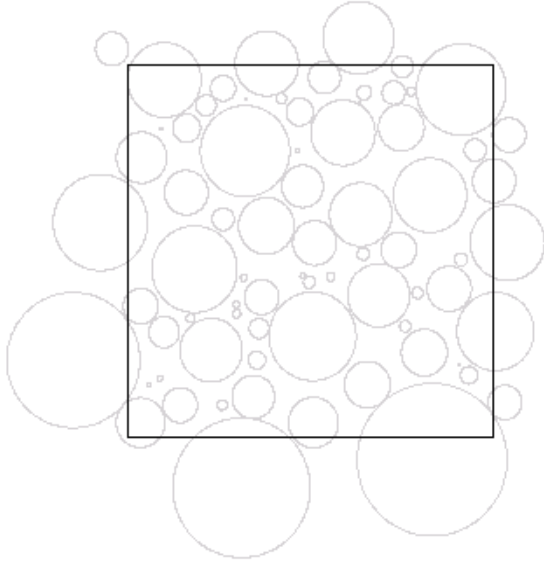


Figure 2: Circles (grey) are placed into a box (black) and along its boundary.

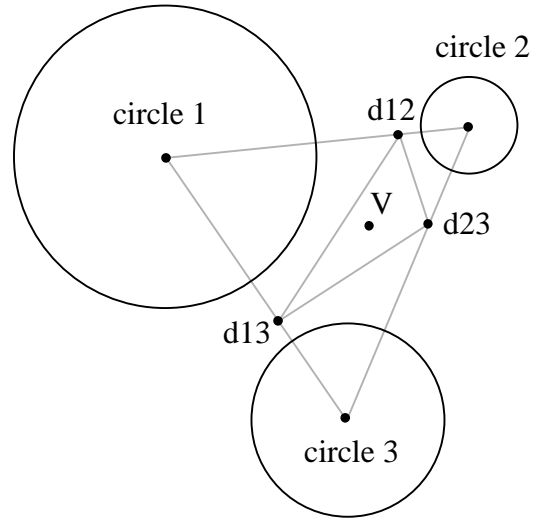


Figure 3: Construction of 'modified' Voronoi points after Delaunay triangulation.

In a second step we define circles by the generated diameters and place this circles, starting with the largest one, into a box that defines the polycrystal RVE on the mesoscale. In order to take into account that grains at the RVE boundary can be positioned partially outside, the circle centers can be placed up to a distance of $d/2$ outside the box (Figure 2). By this condition the maximum area \bar{A} that is taken into account for circle placement can be approximated by:

$$\bar{A} = (l_x + d_{50})(l_y + d_{50}), \quad (5)$$

wherein l_x and l_y are the length dimensions of the two dimensional RVE. However, the area that can be filled by circles is smaller than \bar{A} , because the density of circles in the box is limited. Hence, the diameter generation stops when the sum of circle areas, belonging to diameters d_j , is larger than a specified limit $f \cdot \bar{A}$:

$$\sum \frac{\pi}{4} d_j^2 \geq f \cdot \bar{A}. \quad (6)$$

The limit of Equation (6) should be reasonable defined to guaranty, that all circles can be placed into the box and surrounding band of $d/2$, respectively. A suitable value for the factor f in the following examples was $f = 0.9$. However, it strongly depends on the standard deviation of grain size distribution.

In a third step a Delaunay triangulation of the center points is computed. Based on that triangulation we calculate the positions of 'modified' Voronoi points for each triangle following Figure 3. Assuming a triangle (123) is constructed by the center points of circles 1 to 3. Firstly each triangle edge is divided into two parts proportional to the relation of radii belonging to the circles of edge vertices. Exemplary the edge connecting the center points of circles 1 and 2 is divided by the division point d_{12} at a distance of l_1 :

$$l_1 = \frac{r_1 l}{r_1 + r_2} \quad (7)$$

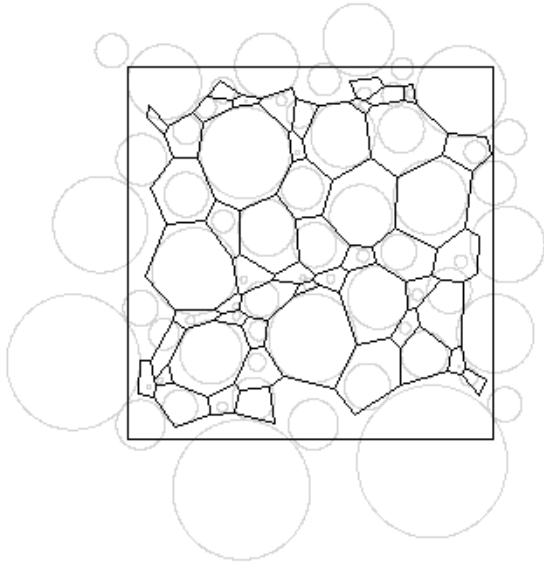


Figure 4: Inner cell structure.

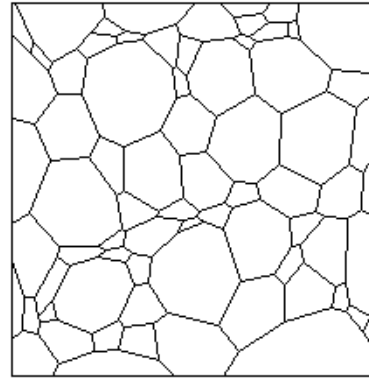


Figure 5: Completed cell structure.

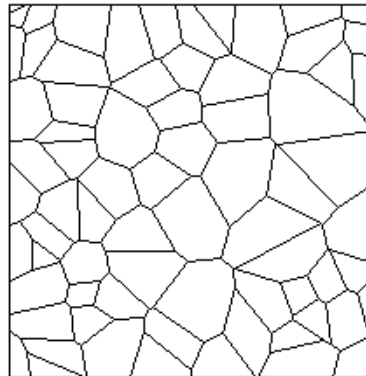


Figure 6: 'Classical' Voronoi cell diagram.

from circle center 1 to circle center 2. l is the distance between center points of circles 1 and 2. r_1 and r_2 are the radii of circles 1 and 2. Secondly the edge division points d_{12} , d_{23} and d_{13} of triangle (123) define a new triangle for which we compute the centroid marked by point V in Figure 3. Point V is the 'modified' Voronoi point of triangle (123).

In a fourth step all 'modified' Voronoi points inside the box are connected according to a 'classical' Voronoi procedure (Figure 4). The resulting structure includes open cells along the boundary.

Finally we connect the open cells with the box boundary in a way, that the added cell edges are perpendicular to connecting lines between neighboring circle centers. Figure 5 illustrates a finished 'modified' Voronoi cell diagram. A comparison with the 'classical' Voronoi cell diagram in Figure 6 shows significant differences especially with respect to the grain size distribution.

The circles in the box do not fill the complete area of the cell structure. This results in a modified grain size distribution of the final cell structure compared to the initial size distribution of circles. Consequently we have to adapt the free parameters of the distribution function, which has been used to generate the circle diameters d_j to obtain a cell structure corresponding with a predefined grain size distribution. Exemplary, a cell structure with median value $d_{50} = 0.94 \mu\text{m}$ and standard deviation $\sigma_d = 0.78$ as measured in thin layer

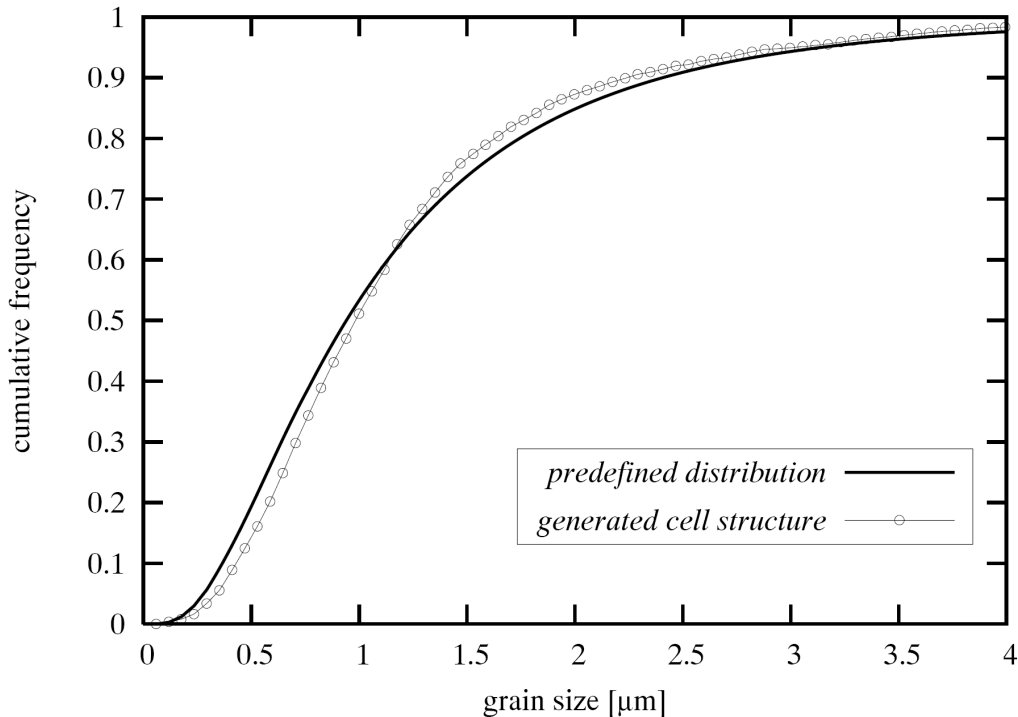


Figure 7: Comparison of predefined cumulative lognormal distribution function and resulting grain size distribution of generated cell structure.

aluminum by [6] shall be generated. In order to obtain this cell structure we generate the circle diameters according to a cumulative lognormal distribution function with adapted values $\bar{d}_{50} = 0.66 \mu\text{m}$ and $\bar{\sigma}_d = 1.40$. The parameters are adapted by an iterative fitting procedure. The resulting grain size distribution shows good agreement with the predefined cumulative lognormal distribution function (Figure 7). An example of the generated cell structure is illustrated in Figure 5. In principle it is possible to reproduce any arbitrary grain size distribution with high accuracy by the proposed algorithm.

3 MATERIAL MODELS ON MESOSCALE

In the next step the grains are discretized by triangular finite elements with quadratic shape functions. Additionally 6 node interface elements are assigned to the boundaries between single grains. Following Iesulauro and Ingrassia [1-3] we apply an orthotropic material model to the grain elements and a coupled cohesive zone model to the interface elements.

3.1 Grains

In order to take into account the dependency of material properties on crystal orientation, an orthotropic linear elastic material model and alternatively an orthotropic elastic plastic material model is assigned to the single crystals. However, the extension to the elastic plastic material model with realistic plasticity properties taken from [1] has shown no relevant improvements compared to the linear elastic model. The material properties required to describe the orthotropic linear elastic material behavior in the plane stress case are the Young's modules E_1 and E_2 , the Poisons ratio ν_{12} , and the shear modulus G_{12} . In the case of plastic behavior we implemented a flow of Hill plasticity with additional parameters of yield stress. The crystal orientation in plane is defined by a random angle $0 \leq \beta \leq \pi$ as illustrated in Figure 8.

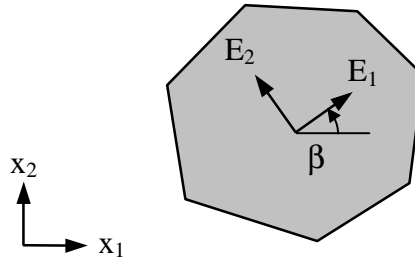


Figure 8: Application of orthotropic material model to grains.

3.2 Grain Boundaries

In order to simulate crack propagation we apply a coupled cohesive zone model (CCZM) on the interface along grain boundaries (Figure 9). Therein the peak strength t_p of the CCZM depends directly on the misorientation $\Delta\beta$ between neighbouring single crystals:

$$\begin{aligned} \Delta\beta &= \beta_1 - \beta_2 \\ t_p(\Delta\beta) &= t_p^{avg} + \Delta t_p \cdot \cos(4 \cdot \Delta\beta), \end{aligned} \quad (8)$$

where β_1 and β_2 indicate the orientations of two crystals along a common boundary. t_p^{avg} is the average value of peak strength and Δt_p the maximal peak strength deviation. The applied CCZM is sufficiently defined by the initial normal stiffness k_n , the peak strength t_p , the localized fracture energy G_f , and the ratio between critical interface openings δ_n^c in normal direction and δ_t^c in tangential direction [9]. The coupling of the interface opening in normal direction δ_n and the relative tangential slip of the two interface surfaces δ_t is realized by the introduction of a relative displacement λ according to Tvergaard [10]. The relation for λ is given in Figure 9.

4 EXAMPLES

As a first example we investigated a displacement controlled tensile tests on a two dimensional polycrystalline structure of aluminum, following Iesulauro [1], to evaluate our model. Therefor we generated 'classical' Voronoi cell structures as used in [1]. Boundary conditions and geometrical dimensions of polycrystal RVE are represented in Figure 10. We

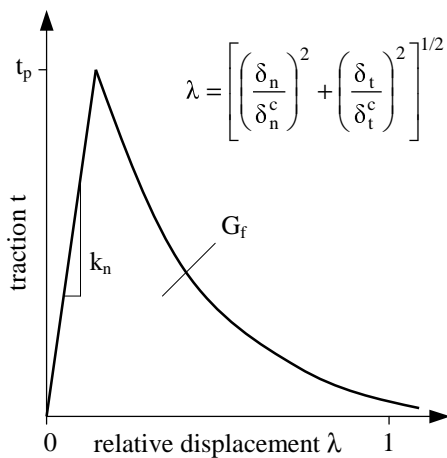


Figure 9: Coupled cohesive zone model.

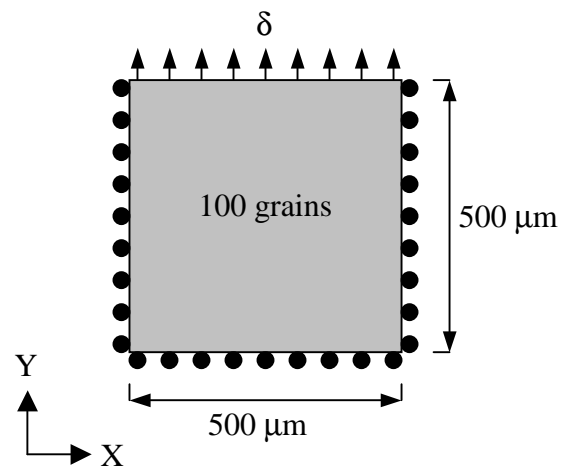


Figure 10: Conditions of tensile test.

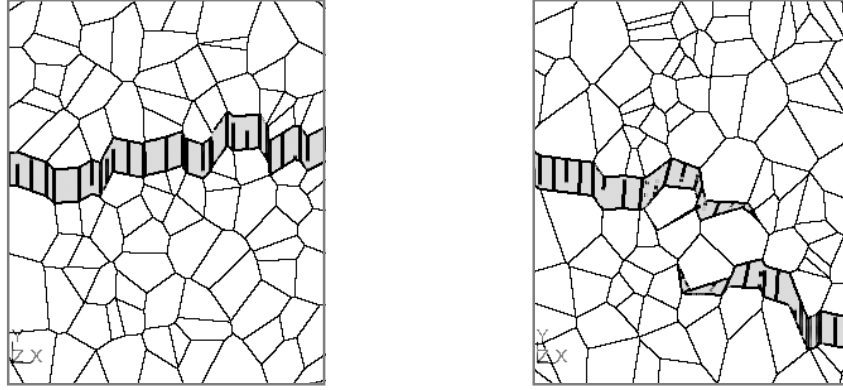


Figure 11: Two representative examples of simulated crack propagation: illustrated is the deformed state at 1% strain. Cracks (grey) are indicated by interface opening. The polycrystal cell structure is generated by the 'classical' Voronoi algorithm.

applied the same material properties to single crystals as in [1] using the orthotropic linear elastic model. In the numerical analysis both, crystal orientation and material properties of each crystal are distributed by normal distribution. Our CCZM differs from the one that was used in [1] only by a more complex decohesion path. However, the material properties are chosen similar. All parameter values needed for the tensile test are summarized in Table 1. The standard deviation σ_d is applied to Young's modules E_1 and E_2 , as well as to the shear modulus G_{12} .

crystals	interfaces
$mean E_1 = 72000 MPa$	$t_p^{avg} = 500 MPa$
$mean E_2 = 42000 MPa$	$\Delta t_p = 0.05 t_p^{avg}$
$mean G_{12} = 72000 MPa$	$k_n = 4e7 MPa$
$\sigma_d = 0.05$	$G_f = 0.15 N/mm$
$\nu_{12} = 0.33$	$\frac{\delta_n^c}{\delta_t^c} = 1$
$0 \leq \beta \leq \pi$	

Table 1: Material and stochastic parameters of tensile test on aluminum samples.

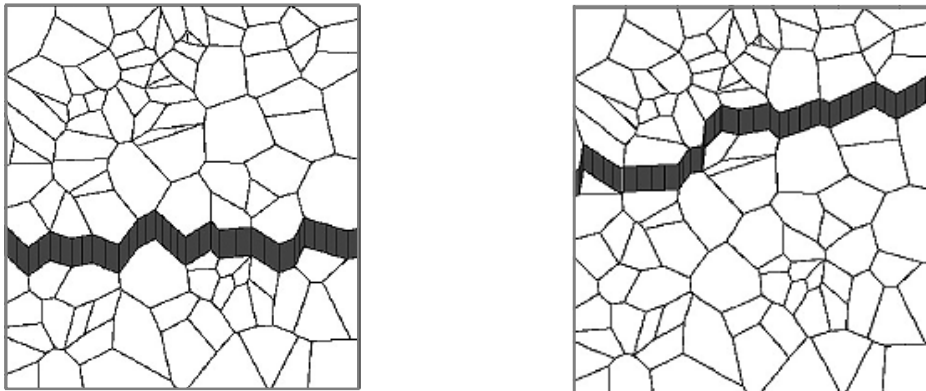


Figure 12: Two examples of simulated crack propagation on the mesoscale published in [1] by Iesulauro.

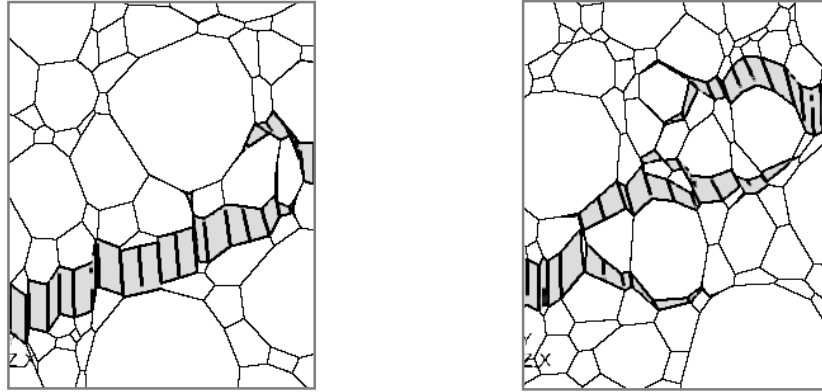


Figure 13: Two representative examples of simulated crack propagation: illustrated is the deformed state at 1.5% strain. Cracks (grey) are indicated by interface opening. The polycrystal cell structure is generated by the 'modified' Voronoi algorithm.

The tensile test was applied to initially undamaged samples. Figure 11 shows two representative results of the deformed polycrystalline structure after tensile test. The crack initiation and propagation is reproduced by an opening of the interface. The complexity of crack formation in our simulations depends on both, the geometry of cell structure as well as the distribution of material parameters and crystal orientation. The mean value σ_t^{poly} of the effective tensile strength calculated by 100 RVE samples is $\sigma_t^{poly} = 442$ MPa. Therewith σ_t^{poly} is lower than the average peak strength of the CCZM and yields a value which is reasonable. Altogether we can conclude that our simulations qualitatively match the results of Iesulauro [1]. For comparison Figure 12 gives an account of two examples simulated by Iesulauro [1].

In a second study we investigated the damage behavior of aluminum samples generated by the 'modified' Voronoi algorithm with a lognormal grain size distribution. The free parameters of the predefined lognormal distribution were chosen according to [6]: $d_{50} = 0.94$ μm and $\sigma_d = 0.78$. Consequently the sample size was adapted to 10 μm in relation to the decreased grain size compared to the preceding example. The principle boundary and loading conditions remained unchanged as well as the material properties (Table 1). First simulations using the more realistic polycrystal structure have shown a higher complexity in crack formation (Figure 13). Additionally the effective tensile strength of the RVE is decreased by approximately 5%-10%.

5 OUTLOOK TO MICROSCALE

The future research work is focused on the determination of constitutive relations for the CCZM from mixed continuum atomistic simulations performed on a RVE on the microscale and subsequential homogenization of these results to mesoscale processes. Therefor, we have done first investigations of atomic debonding along grain boundaries based on the quasicontinuum (QC) method mainly developed by Tadmor, Miller and Ortiz [4,11,12]. Based on atomistic energy laws this method allows a reproduction of atomic debonding as the source of micro crack initiation in zones of localized damage. In undamaged model regions conventional continuum mechanical formulations are applied to calculate the structural response. During the simulation zones of atomistic resolution are adapted following the process of damage. Therewith the method allows a significant reduction of degrees of freedom compared to pure atomistic methods and ensures a high accuracy on the atomic level at the same time.

An example of a displacement controlled tensile test on grain boundary samples using the QC method is given in Figure 14. The atomic positions along grain boundary in fcc aluminum

are plotted in (a) and (c) corresponding to the deformation states indicated in the response path (b). The QC program used for the simulations is freely available on the QC website [13]. Important limitations of this program are the restrictions to 2D and to zero temperature. Hence further developments are necessary to apply the QC method to realistic simulations of polycrystal materials. However, the theory of 3D QC method is well developed [14] and first extensions to finite temperature QC already have been published [15,16].

6 CONCLUSIONS

The proposed polycrystal model enables us to analyze the crack formation in statically loaded two dimensional polycrystalline mesostructures of metal materials without the necessity of initial damage definition as necessary in classical fracture mechanic approaches. A main advantage of our meso model is the underlying realistic polycrystal structure. This structure shows a better fit to measured grain size distributions in metal materials compared to the often used 'classical' Voronoi diagrams. In principle we are able to reproduce polycrystal structures with arbitrary predefined grain size distributions by the presented 'modified' Voronoi algorithm.

However, up to now the improved model is limited to two dimensions and can not cover effects of damage evolution in 3D. Hence, the current work is concentrated on the extension of the introduced polycrystal model to three dimensions. Therefor these theories are available and have to be applied to practical problems.

Furthermore the future research work has to focus on the development of a 3D mixed continuum atomistic model on the microscale at finite temperature to realistically simulate the atomic debonding along grain boundaries and homogenize the material behavior of micro RVE to describe the decohesion on the mesoscale.

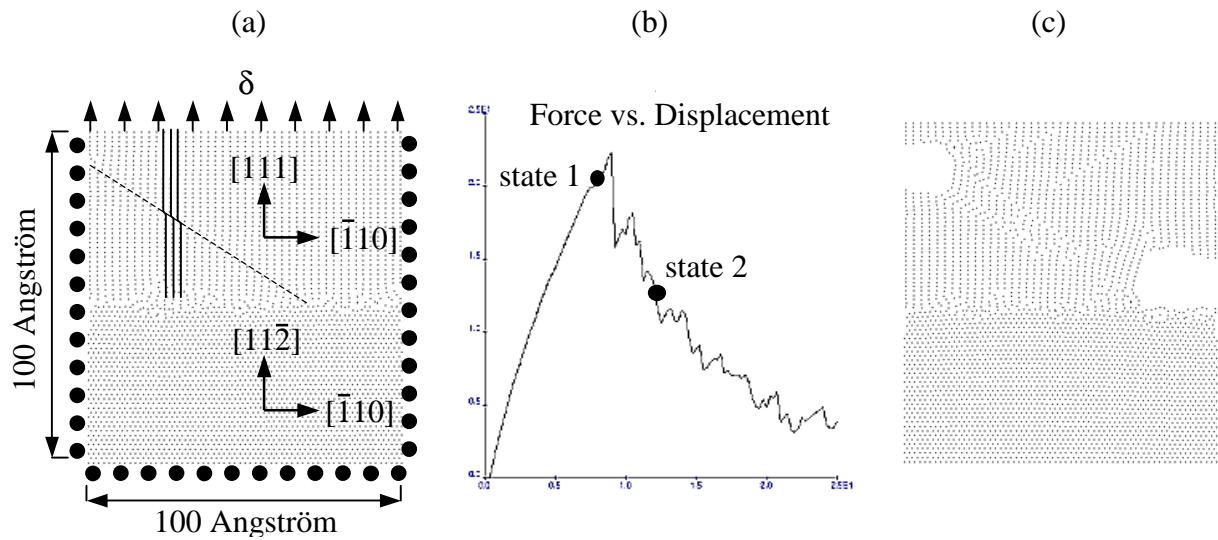


Figure 14: Simulation of atomic debonding along grain boundary by QC method: (a) Boundary and loading conditions of displacement controlled tensile test and formation of dislocation in state 1. (b) Force vs. displacement diagram indicating state 1 and state 2. (c) Deformed grain boundary structure in state 2 (atomic positions).

REFERENCES

- [1] E. Iesulauro, *Decohesion of Grain Boundaries in Statistical Representations of Aluminium Polycrystals*. Master Thesis, Cornell University, 2002.
- [2] E. Iesulauro, A. R. Ingraffea, S. Arwade and P. A. Wawrzynek, Simulation of Grain Boundary Decohesion and Crack Initiation in Aluminium Microstructure Models. W. G. Reuter and R. S. Piascik eds. *Fatigue and Fracture Mechanics: 33rd Volume*, ASTM, West Conshohocken, PA, 2002.
- [3] A. R. Ingraffea, E. Iesulauro, K. Dodhia and P. A. Wawrzynek, A Multiscale Modeling Approach to Crack Initiation in Aluminium Polycrystals. H. A. Mang, F. G. Rammerstorfer and J. Eberhardsteiner eds. *Fifth World Congress on Computational Mechanics*, WCCM V, Vienna, Austria, 2002.
- [4] E. B. Tadmor, M. Ortiz and R. Phillips, Mixed Atomistic and Continuum Models of Deformation in Solids. *Langmuir*, **12**, 4529-4534, 1996
- [5] F. Aurenhammer, Voronoi Diagrams – A Survey of a Fundamental Geometric Data Structure. *ACM Computing Surveys*, **23**(3), 345-405, 1991
- [6] S. Kirchner, *Ausscheidungshärtung dünner Al-0,6Si-0,6Ge-Schichten: Studie zur Übertragbarkeit eines Massivmaterial-Legierungskonzeptes*. Dissertation, University Stuttgart, 2001
- [7] C. V. Thompson, Grain Growth in Thin Films. *Annual Review of Materials Science*, **20**, 245-268, 1990
- [8] W. Fayad, C. V. Thompson and H. J. Frost, Steady-State Grain-Size Distributions Resulting from Grain Growth in Two Dimensions. *Scripta Materialia*, **40**(10), 1199-1204, 1999
- [9] J. F. Unger and C. Könke, Simulation of concrete using the Extended Finite Element Method. N. Bicanic, R. de Borst, H. Mang, and G. Meschke eds. *Proceedings of EURO-C 2006, Computational Modelling of Concrete Structures*, 2006
- [10] V. Tvergaard, Cohesive zone representations of failure between elastic or rigid solids and ductile solids. *Engineering Fracture Mechanics*, **70**, 1859-1868, 2003
- [11] R. E. Miller and E. B. Tadmor, The Quasicontinuum Method: Overview, applications and current directions. *Journal of Computer-Aided Materials Design*, **9**, 203-239, 2003
- [12] E. B. Tadmor and R. E. Miller, The Theory and Implementation of The Quasicontinuum Method. S. Yip ed. *Handbook of Materials Modeling*, **1**, Kluwer Academic Publishers, 2005
- [13] www.qcmethod.com/ *The Quasicontinuum Website*
- [14] J. Knap and M. Ortiz, An Analysis of the quasicontinuum method. *Journal of the Mechanics and Physics of Solids*, **49**, 1899-1923, 2001
- [15] V. Shenoy, V. Shenoy and R. Phillips, Finite Temperature Quasicontinuum Methods. V. V. Bulatov ed. *Multiscale modelling of materials*, 465-472, 1999
- [16] L. M. Dupuy, E. B. Tadmor, R. E. Miller and R. Phillips, Finite Temperature Quasicontinuum: Molecular Dynamics without all the Atoms. *Physical Review Letters*, **95**, 2005